INTERFACE

royalsocietypublishing.org/journal/rsif

Research

Cite this article: Dutta R, Mandal S, Lin H-CA, Raz T, Kind A, Schnieke A, Razansky D. 2020 Brilliant cresyl blue enhanced optoacoustic imaging enables non-destructive imaging of mammalian ovarian follicles for artificial reproduction. *J. R. Soc. Interface* **17**: 20200776.
http://dx.doi.org/10.1098/rsif.2020.0776

Received: 23 September 2020
Accepted: 9 October 2020

Subject Category:
Life Sciences–Engineering interface

Subject Areas:
biomedical engineering, biotechnology, biochemistry

Keywords:
brilliant cresyl blue, optoacoustic imaging, artificial reproductive technology, medical imaging, veterinary medicine

Authors for correspondence:
Rahul Dutta
e-mail: rahul.dutta@mail.huji.ac.il
Subhamoy Mandal
e-mail: s.mandal@tum.de

†These authors contributed equally to the study.

Electronic supplementary material is available online at rs.figshare.com.

THE ROYAL SOCIETY PUBLISHING

Brilliant cresyl blue enhanced optoacoustic imaging enables non-destructive imaging of mammalian ovarian follicles for artificial reproduction

Rahul Dutta[1,†], Subhamoy Mandal[2,3,†], Hsiao-Chun Amy Lin[2,4], Tal Raz[1], Alexander Kind[5], Angelika Schnieke[5] and Daniel Razansky[2,6]

[1]Koret School of Veterinary Medicine, The Robert H. Smith Faculty of Agriculture, Food and Environment, Hebrew University of Jerusalem, Israel
[2]Institute for Biological and Medical Imaging, Helmholtz Center Munich, Neuherberg, Germany
[3]Department of Electrical and Computer Engineering, Technical University of Munich, Germany
[4]iThera Medical GmbH, Munich, Germany
[5]Chair of Livestock Biotechnology, Technical University of Munich, Germany
[6]Institute for Biomedical Engineering and Institute of Pharmacology and Toxicology, University of Zurich and ETH Zurich, Switzerland

RD, 0000-0003-2918-9591; SM, 0000-0002-6032-554X; H-CAL, 0000-0002-1393-369X; AS, 0000-0002-5761-9635; DR, 0000-0001-8676-0964

In the field of reproductive biology, there is a strong need for a suitable tool capable of non-destructive evaluation of oocyte viability and function. We studied the application of brilliant cresyl blue (BCB) as an intra-vital exogenous contrast agent using multispectral optoacoustic tomography (MSOT) for visualization of porcine ovarian follicles. The technique provided excellent molecular sensitivity, enabling the selection of competent oocytes without disrupting the follicles. We further conducted *in vitro* embryo culture, molecular analysis (real-time and reverse transcriptase polymerase chain reaction) and DNA fragmentation analysis to comprehensively establish the safety of BCB-enhanced MSOT imaging in monitoring oocyte viability. Overall, the experimental results suggest that the method offers a significant advance in the use of contrast agents and molecular imaging for reproductive studies. Our technique improves the accurate prediction of ovarian reserve significantly and, once standardized for *in vivo* imaging, could provide an effective tool for clinical infertility management.

1. Introduction

The term 'ovarian reserve' is used to describe a woman's reproductive potential, specifically, the capacity of the ovary to produce oocytes that are capable of fertilization resulting in a healthy and successful pregnancy [1]. It is a complex clinical phenomenon influenced by multiple factors such as age, genetics and the health of the female, as well as environmental factors. Ovaries undergo irreversible decline of the oocyte reserve starting from the birth of the female, eventually ending in menopause at a later age. Accurately predicting the rate of decline remains a challenging question for researchers and clinicians. Currently, the tests for ovarian reserve in the clinical setting include both biochemical tests, such as measuring follicle stimulating hormone and anti-Müllerian hormone blood concentrations, as well as ultrasonographic imaging of the ovaries; however, they serve only as a proxy for oocyte quantity and are considered poor predictors of oocyte quality [1]. Thus, medical imaging technologies have slowly emerged as an indispensable component of artificial reproductive technology (ART) for the management of infertility [2]. Existing diagnostic imaging technologies, such as pelvic magnetic resonance imaging and ultrasonic imaging, have provided valuable insights into the mammalian

reproductive system. Ultrasonographic follicular imaging, the primary tool for oocyte retrieval for *in vitro* fertilization (IVF) and embryo culture, reveals the growing follicle only as a hypoechoic structure (black bubble) and is lacking the resolution required to image the oocyte [3]. Folliculometric information, such as follicular wall thickness, is determined by manual or semi-automated segmentation and provides only crude information with questionable predictive value [4]. Thus, the determination of oocyte quality is vital in assisted reproduction, but there has not yet been any assessment method that does not disrupt the follicle structure. Therefore, researchers and clinical practitioners are in urgent need of a non-invasive innovative imaging method that reliably predicts oocyte viability and developmental competence. Such methods would be of great benefit for reproductive biologists and clinicians using ART, and potentially can revolutionize female reproductive health management, in humans and animals.

The study aims to establish brilliant cresyl blue (BCB) [5] as a contrast agent for non-destructive evaluation of oocyte quality. But contrast enhancement for imaging interventions using BCB has so far not been attempted in ovarian follicle imaging. A favourable toxicity profile, relative ease of use and inexpensive nature makes BCB an ideal candidate for a contrast agent.

BCB is a supravital stain, commonly used for counting reticulocytes [6]. BCB also has previously been used effectively to identify developmentally competent oocytes without compromising oocyte viability [7–10]. BCB is reduced by the intracellular activity of glucose-6-phosphate dehydrogenase (G6PDH), a pentose phosphate pathway enzyme, the activity of which gradually decreases as oocytes reach the growth phase [11]. Accordingly, oocytes in the mature growth phase do not reduce BCB and exhibit a blue-coloured cytoplasm (BCB +ve); while growing oocytes have a high level of G6PDH activity, resulting in a colourless oocyte cytoplasm (BCB −ve) [12]. Multispectral optoacoustic tomography (MSOT) was employed as a molecular imaging method capable of selectively quantifying the distribution of specific biomarkers using multiple excitation wavelengths and delivers optical contrast at unprecedented resolution and penetration depths [13,14]. The method has previously been applied to image fluorescent proteins in model organisms [15], and for tracking perfusion profiles of contrast agents and blood oxygenation *in vivo* [16]. MSOT uses non-ionizing radiation (near-infrared range) with safe levels of optical flux (less than 15 mJ pulse^{-1} on the surface of the imaged tissue), making it attractive for non-destructive cellular imaging. However, the use of optoacoustic for imaging reproductive cell has been limited. Viator *et al.* used photoacoustic flowmetry to detect sperm samples in a dilute solution [17], and Wittmann *et al.* employed MSOT to study blood–testis barrier. To the best of our knowledge, the current study provides the first experimental results of non-destructively imaging viable oocytes from mammalian sources.

We conducted the imaging trials *in vitro* by injecting BCB into porcine ovarian follicles and imaging the intact ovarian structure *ex vivo*. Spectral unmixing [18] and image analysis techniques [19] were used on acquired MSOT images to quantify image contrast and identify suitable follicles with competent oocytes. The MSOT results were further validated using a state-of-the-art selective plane illumination microscopy (SPIM) tool. In this way, both the anatomy and contrast agent distribution [20] were visualized, gaining precise folliculometric information, including volume, anatomical position, structural details and oocyte size. To investigate whether the procedure is toxic to the oocytes in any way, oocytes from the tested follicles were isolated and cultured *in vitro* then analysed by real-time and reverse transcriptase polymerase chain reaction (RT-PCR) and DNA fragmentation analysis.

The results conclusively prove that the administration of BCB and MSOT imaging do not impact the viability of reproductive units, i.e. oocytes. Our experimentations support the usefulness of BCB-enhanced MSOT imaging as a simple, gentle and efficient translational imaging method of monitoring oocyte viability. Thus, the current study opens up new possibilities for workflow optimization and risk-mitigation in ART.

2. Experimental methods and results

2.1. Spectral evaluation of brilliant cresyl blue and experimental protocol for imaging of follicles

A commercial MSOT system (inVision 256TF, iThera Medical GmbH, Munich, Germany) was used to probe a narrow window of BCB contrast in the near-infrared range (wavelengths 680–900 nm). Given the inherent noise and low contrast in *ex vivo* imaging samples, we employed non-negative constrained model-based image reconstruction [21,22] and automatic calibration methods [23] to improve image quality. Recent studies have shown that the optoacoustic spectrum is often not correlated to the absorption spectrum of chromophores. Additionally, Luke *et al.* have shown that ≥ 5 wavelengths are required to have a stable concentration estimate of a chromophore during spectroscopic optoacoustic imaging [24]. As described previously [25], we diluted a 13 mM stock solutions of 1 M BCB in Dulbecco's phosphate-buffered saline (DPBS) to six working concentrations (25 × to 250 × dilutions). We used 10 wavelengths to derive the reference optoacoustic spectrum for BCB at the designated concentrations [26]. An automatic segmentation and tracking algorithm developed in-house [19] was used to automatically annotate the region of interest (ROI) (approximately 25 ± 2 pixels) in real time and 50 frame averaging was done to achieve high signal-to-noise ratio. As illustrated in figure 1, optoacoustic spectral evaluation revealed that 260 µM (50 times dilution) BCB provided satisfactory signal recovery without quenching. This concentration was subsequently used throughout the experimentation and imaging trials. Figure 2 illustrates the phases in the entire ovarian imaging protocol (5 phases) standardized for the study. Ovarian follicles were first injected with BCB solution using a fine bore needle (31G). Follicles contain follicular fluid that further dilutes BCB, so injection concentrations were conservatively overestimated by 10% volume (figure 2.1). The ovaries were then placed on a polyethylene sheet supplied with DPBS solution and placed in the imaging domain submerged in deionized water at 34°C for the MSOT imaging (figure 2.2). In figure 2.3, the single-wavelength image acquired at 690 nm shows the internal anatomy of the extracted ovary after the injection of BCB. To clearly identify the locations where BCB is deposited relative to tissue morphology, we spectrally unmixed the MSOT signals into two channels (BCB and tissue). The BCB channel showed deposition along the walls of the follicles (figure 2.3—spectrally resolved image). We used five different wavelengths (680 nm, 690 nm, 700 nm, 710 nm and 850 nm) to acquire the spectral dataset. A vertex-component analysis-based blind spectral unmixing

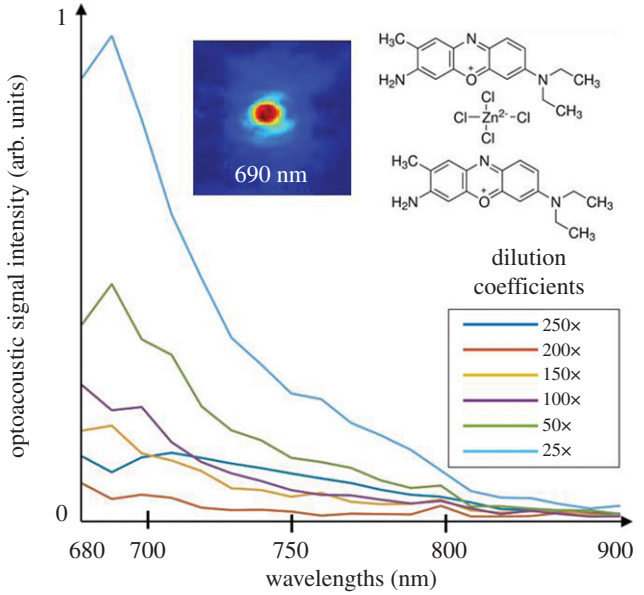

Figure 1. Wavelength-dependent optoacoustic signal extinction curve for BCB. The optoacoustic signal responses are measured at several pre-injection dilution coefficients ($x = 13$ mM stock solution of BCB/DPBS) using the MSOT (cross-sectional) imaging at varying wavelengths. The BCB solution was perfused through a transparent fine bore polyurethane tubing (0.86 mm ID and 1.27 mm OD) embedded inside a scattering agar block (7% intralipid by volume). The signal values were determined by fitting an ROI and computing the mean image intensity across the ROI, each for corresponding wavelengths (20 wavelengths were recorded) and dilution coefficients. A representative reconstruction of a cross-sectional image is shown as an inset.

algorithm [27] was used to isolate the location of the BCB chromophores. The individual follicles were isolated and the cumulus-oocyte complexes (COCs) manually extracted and visually evaluated by optical microscopy. Figure 2.4 shows the microscopic images of COCs graded for validation of the results. We have also developed automated oocyte grading algorithms based on machine learning techniques [28,29], but full descriptions are beyond the scope of this account. In the final stage of the workflow, we attempted *in vitro* embryo culture of irradiated oocytes (figure 2.5) to ascertain viability.

In figure 3*a*, we show the unmixed BCB channel and the site of extraction of the chosen oocyte (inset marked with box). However, looking at a two-dimensional frame does not provide correct size estimate of the follicle. Thus, we included the three-dimensional rendering of the full ovarian mass by stacking multiple scan slices along the Z-direction scanned at a distance of 0.1 mm (figure 3*b*). The three-dimensional scan provides suitable anatomical landmarks and allows the computation of follicular volume, an important marker of maturity as corroborated by SPIM measurements (electronic supplementary material, figure S1). A flyby video of cross-sections of the entire ovary is shown in movie 1 (frames: 160, step size: 0.1 mm, obtained at 720 nm at 34.1°C). Fast scanning protocols (approx. 5 min/ovarian sample) with 10 Hz laser pulsation were employed, the laser irradiation on the surface of ovaries is 12–20 mJ/pulse (wavelength dependent). The values are below the maximum permissible limits (MPE) for *in vivo* small animal imaging.

Ovaries were scanned before (pre-injection) and after (post-injection) the BCB was injected. We observed a clear increase of signal along the walls of the follicles post-injection, as illustrated by figure 4*b*, vis-à-vis the pre-injection image (figure 4*a*). The test was repeated over 12 ovarian samples (approx. 100 follicles). Two ovaries were selected for quantitative evaluation and their relative signal increase was calculated. Figure 4*c* shows box plots of normalized intensities of 15 ROIs chosen in each ovary along the follicle walls for two independent ovarian samples. In both cases, the intensity of optoacoustic signal from the post-injection image was higher than pre-injection image of ovaries, considering the images were acquired at 690 nm laser wavelength, i.e. highest absorption of BCB in the probed optical spectrum. In the pre-injection sample, the follicles are barely visible; however, the residual blood in bigger vessels shows up as bright contrast (figure 4*a*). Thus, we chose suitable ROI (around the follicles) instead of taking the mean intensity value of the images, to avoid erroneous quantification from the presence of residual blood. The spread of contrast values post-injection was higher compared to pre-injection, due to the different levels of hormones and follicular volumes (figure 4*b*). The detailed scatter plot (electronic supplementary material, figure S2) shows the intensities before and after injection of each ROI. Close observation revealed that some ovarian follicles show no significant changes in contrast even after injection; these are developing follicles that decolourize the BCB contrast. These BCB −ve follicles were thus rejected, and oocytes were not extracted from them for further development.

2.2. Validation of multispectral optoacoustic tomography imaging using histology and SPIM studies

The MSOT system used was limited to 150 µm in-plane resolution [30], extendable to approximately 120 µm using pixel super-resolution methods [31]. This was optimal for visualizing BCB contrast within follicular masses, but fell short of visualizing the COCs. To validate our observations at higher resolution, a randomly chosen set of MSOT-analysed ovarian follicles were cryosliced (figure 5*a*) for examination using histological methods and SPIM. The inset (red) in figure 5*a* shows the chemically cleared oocyte, figure 5*b* shows the reference MSOT image, figure 5*c* shows the haematoxylin and eosin (H&E) stained image (20 x) and figure 5*d* shows the SPIM image of the intact follicle.

A state-of-the-art SPIM system [32] (electronic supplementary material, figure S1a) was fabricated in-house to enable ovarian follicular imaging. A wide range of individual follicles were extracted from two different sets of ovaries and all selected samples were imaged in their entirety, as their sizes matched the camera field of view. The SPIM imaging requires sample transparency, which was achieved via a time-consuming chemical clearing protocol to render the samples free of optical scattering (see electronic supplementary material for details of the SPIM method). The high contrast-to-noise ratio and image resolution achieved by SPIM readily distinguished the different anatomical features (figure 5*d*). We analysed the most relevant morphological features using the SPIM images, i.e. size of the developing COC and follicle wall thickness. The COC can be clearly seen attached to the inner follicle wall. COCs were detectable in approximately 70% of follicles, and COC size varied between 40 µm and 110 µm (electronic supplementary material, figure S1b/movie S2). Detection of COC as small as 40 µm is comparable to the resolution of histological analysis [33] and surpasses that of ultrasound biomicroscopy [34]. Histological sections obtained through cryoslicing (figure 5*a*)

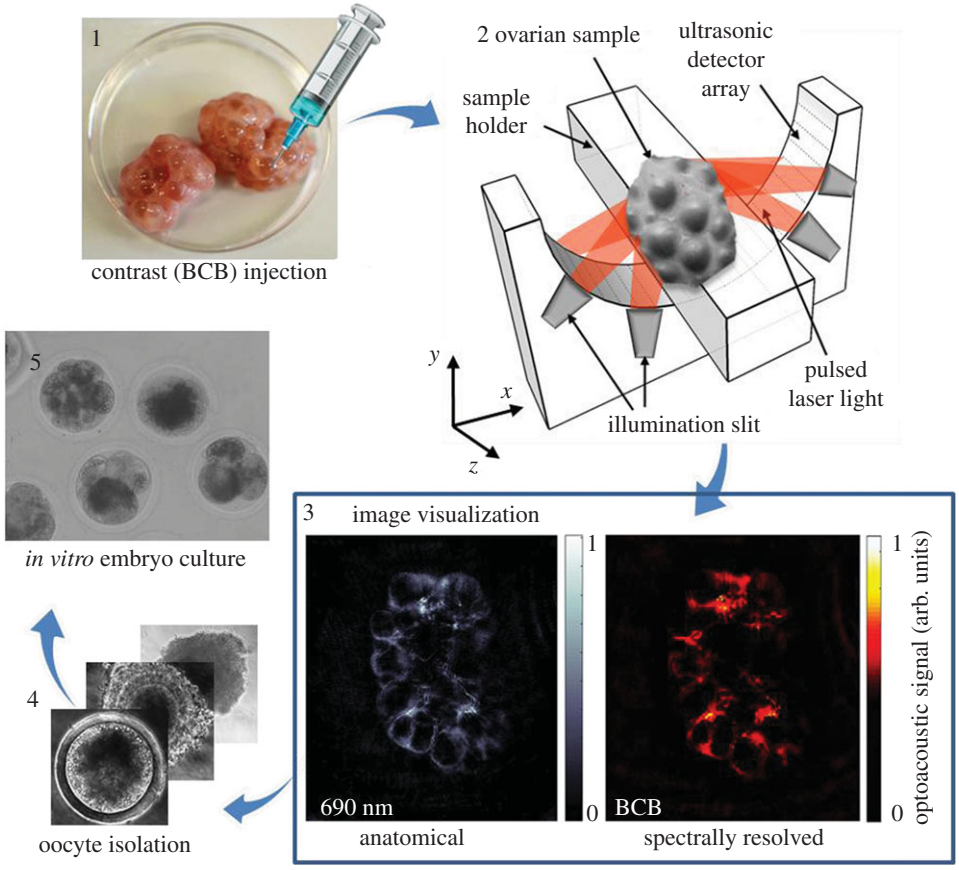

Figure 2. Protocol for ovarian imaging. (1) BCB was injected into the ovarian follicles using an ultrafine needle. (2) After BCB injection, ovaries were imaged using MSOT. (3) Single-wavelength (690 nm) image of BCB contrast-enhanced ovarian follicles shown in anatomical reference image, and the contrast from BCB molecules is spectrally resolved through a blind unmixing process using five wavelengths. (4) Following MSOT imaging, oocytes were isolated by aspiration and kept for further *in vitro* culture and analysis. (5) The final stage shows the successful formation of the embryo from the isolated oocytes extracted from the BCB + MSOT-scanned ovarian follicles.

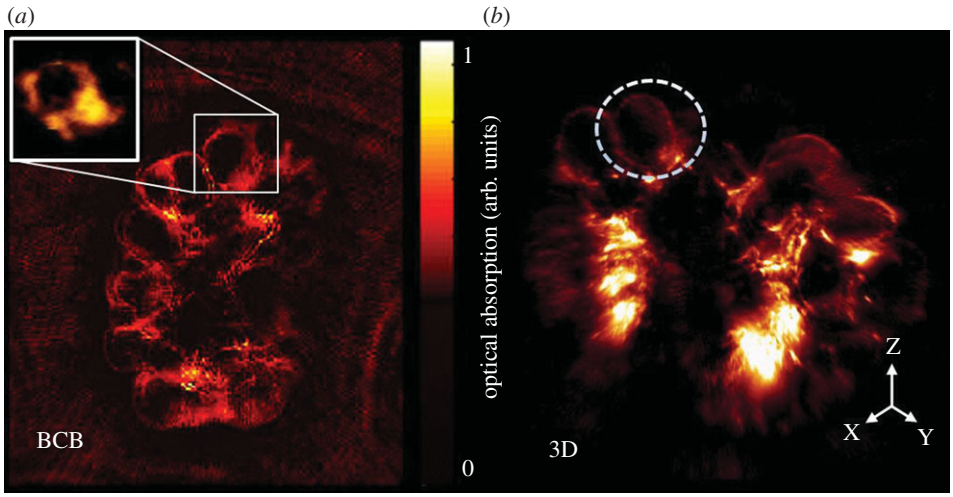

Figure 3. The unmixed BCB channel obtained by using five wavelengths (*a*). The inset shows the original position of the isolated oocyte, and a zoomed in three-dimenional volume rendered version of the selected single oocyte. (*b*) Three-dimensional rendering of entire ovary obtained using *z*-slacking and fast scanning protocols (approx. 5 min/ovarian sample at 10 Hz laser pulsation); approximate position of a single viable oocyte is marked.

and H&E stained microscopic images served as controls (figure 5*c*).

2.3. *In vitro* embryo culture

We examined whether oocyte viability was harmed by laser irradiation from MSOT scanning and BCB staining. Nuclear maturation of each oocyte was scored by attainment of metaphase II, as judged by the presence of condensed chromosomes in an equatorial position and extrusion of the first polar body (figure 6). Nuclear maturation data (table 1) showed no significant difference in nuclear maturation rate between MSOT-scanned and non-scanned control oocytes. The MSOT scanner provides a narrow, but sufficient band of wavelengths to identify signals from competent BCB (+) follicles and distinguish them from the developing follicles. This enabled

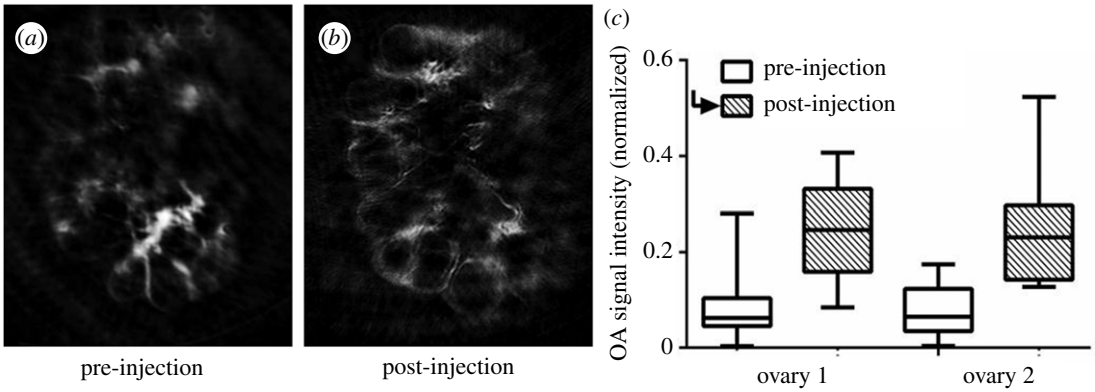

Figure 4. Scan of (intact) ovaries *ex vivo* before (*a*) and after (*b*) injection of BCB (100× diluted 13 mM stock solution) is shown. The post-injection images (normalized) of the ovaries show an increase in relative contrast values. The box plots of contrast values for two ovaries, before and after the injection are shown (*c*). Fifteen (15) data-points in each ovary were chosen for evaluation. Electronic supplementary material, figure S2, shows the scatter plot of the data-points (both before and after injection) for each of the follicles in individual ovaries.

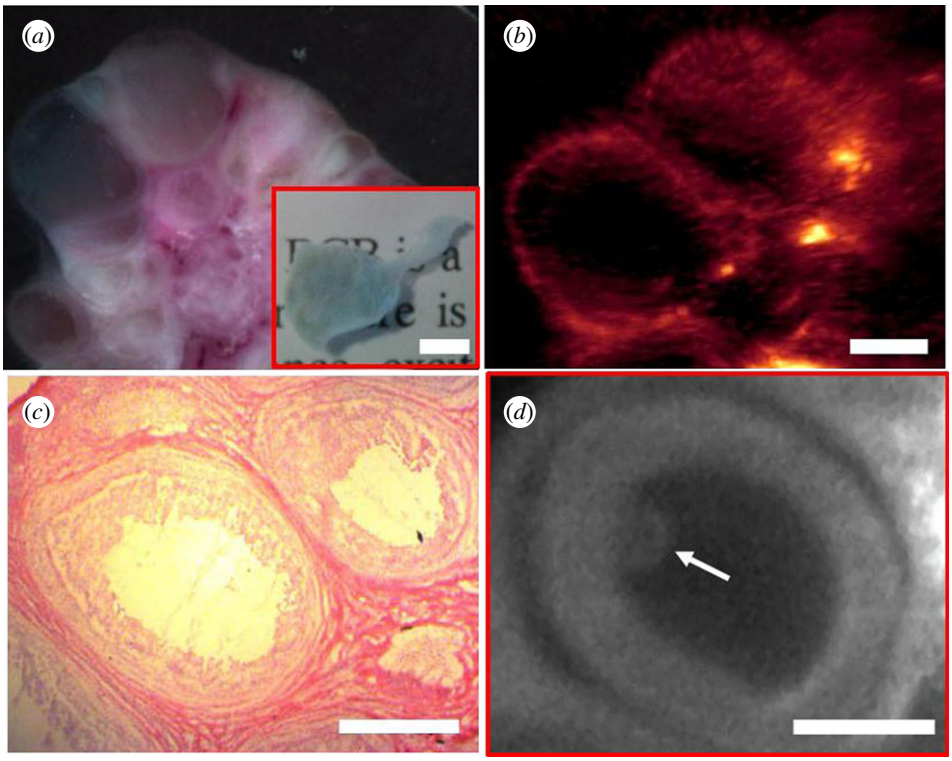

Figure 5. The cryosliced image of BCB+ porcine ovary (*a*), and the optoacoustic image of the selected ovarian section (*b*). The histological evaluation was done using H&E stains (*c*) and validated using the SPIM imaging (*d*). Inset in (*a*) shows an isolated follicle which was cleared and imaged using SPIM to obtain the corresponding anatomy for validation (*d*); the arrow points to the attached COC. Scale bars, *ca* 1 mm.

suitable oocytes to be selected for *in vitro* embryo culture without disrupting follicle structure. To validate the findings, we assessed the competence of oocytes to develop further by culture *in vitro*. Oocytes aspirated from MSOT-scanned ovaries were parthenogenetically activated to indicate developmental potential. Development was scored as the number of embryos consisting of two to eight equally sized blastomeres 48 h after activation. No statistically significant difference was observed between MSOT-scanned BCB +ve oocytes and control BCB +ve oocytes (table 1), indicating that MSOT scanning has no detectable detrimental effect. As expected, nuclear maturation and parthenogenetic activation rates were significantly higher in BCB +ve than BCB –ve oocytes, as reported in goats [35] and heifers [36]. The low nuclear maturation rate of BCB –ve oocytes could be due to incomplete or abnormal cytoplasmic maturation.

2.4. Expression of stress and apoptosis-related genes in brilliant cresyl blue-multispectral optoacoustic tomography scanned porcine cumulus-oocyte complexes

Gene expression analysis of five genes (electronic supplementary material, table S1) chosen for their roles in cell stress and apoptosis was conducted to determine whether BCB staining and irradiation from MSOT scanning is stressful to oocytes. Differential expression of the stress-associated gene *TP53* and three genes related to apoptosis, *BCL*, *BAK* (BCL2-antagonist/killer) and *CASP3* (caspase 3), was analysed by quantitative real-time RT-PCR in two pools of 50 to 60 randomly selected COCs from scanned and control ovaries without considering their developmental competence

Table 1. Nuclear maturation and parthenogenetic activation.

	MSOT scanned		control group	
	BCB +ve	BCB −ve	BCB +ve	BCB −ve
nuclear maturation (%)	85.52 ± 2.92	78.41 ± 3.91	86.48 ± 3.07	79.9 ± 3.82
parthenogenetic activation (%)	88.91 ± 3.65	70.57 ± 3.28	87.98 ± 4.91	69.03 ± 5.26

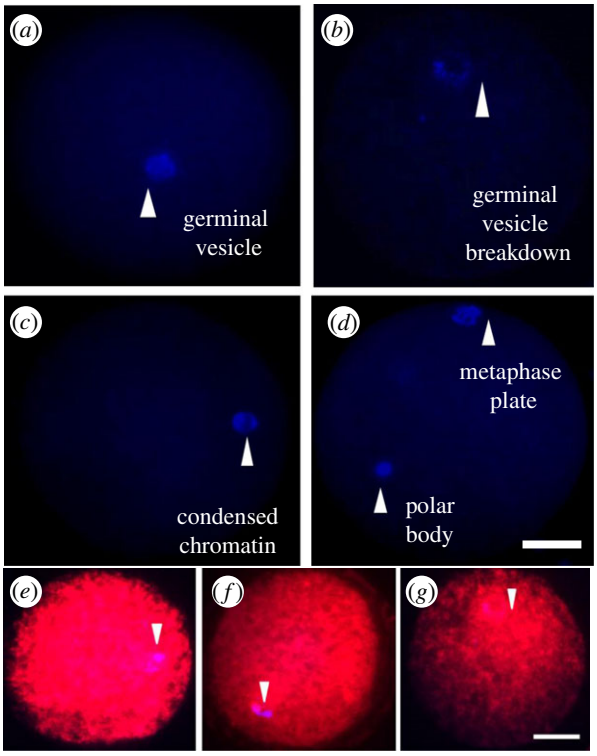

Figure 6. Progression of BCB stained oocytes through different stages of maturation. (*a*) Immature oocyte, (*b*) germinal vesicle breakdown stage, (*c*) appearance of first polar body and (*d*) mature oocyte with visible polar body and metaphase plate. Mitochondrial distribution of (*e*) BCB +ve oocytes showing uniform distribution with polar body and metaphase plate, (*f*) a control oocyte showing uniform distribution with polar body and metaphase plate and (*g*) BCB −ve oocyte arrested at germinal vesicle breakdown stage with non-uniform mitochondrial distribution. All scale bars indicate 100 µm.

(figure 7*a*). Three replicates were conducted for each experiment. Figure 7*b* shows that no significant difference was detected in relative mRNA expression of *TP53*, *BCL*, *BAK* and *CASP 3* ($p < 0.05$), between oocytes isolated from BCB-MSOT-scanned and control ovaries. Studies in humans and mice have revealed a clear relationship between *in vitro* culture-related stress and *TP53* expression in embryos [37]. *BCL XL*, *BAK* and *CASP3* are members of two important regulatory families involved in apoptosis. *BCL XL* and *BAK* are pro-apoptotic members of the Bcl-2 family that induce oocyte apoptosis when cytoplasmic levels are elevated [38].

2.5. DNA fragmentation assay

TUNEL analysis to detect DNA fragmentation was carried out as a further indicator of cell stress and apoptosis, following the protocol described previously [39] (figure 8*a–c*). A TUNEL score was determined as the percentage of COCs showing signs of DNA fragmentation, as indicated by a fluorescent signal. There was no significant difference in TUNEL score between oocytes isolated from BCB-MSOT-scanned ovaries (31.26% ± 4.23) and from control ovaries (30.11% ± 2.97). Though it is not clear whether the BCB test could serve as an indirect marker of oocyte apoptosis, our investigation of the probable effect of MSOT scanning on oocyte quality revealed that it imposed no apparent stress on the oocyte. The average exposure time for each ovary was approximately 25 min, with maximal flux approximately 20 mJ cm^{-2} (per pulse) and an average intensity of 200 mW cm^{-2} at the surface (at 750 nm). Although not directly relevant for our imaging experiments, these per-pulse energy levels and average power of the laser were below the MPE levels for human skin [40]. There exists no regulatory guideline for irradiation of internal organs or reproductive tissue, and researchers commonly determine damages by visual observation or cryoslicing extracted tissue. The histological and SPIM evaluations showed no physical damage to the tissue. Due to extended processing time and exposure of oocytes due to imaging, we also conducted DNA fragmentation checks. We found no evidence of DNA fragmentation in the cumulus layer in immature porcine COCs. This is consistent with a similar finding in cattle where no TUNEL signal was obtained in cumulus cells of immature oocytes [41]. Thus, the DNA fragmentation assay and relative mRNA expression of important apoptosis-related genes indicate that BCB-MSOT scanning does not cause stress to the oocytes.

3. Discussion and conclusion

We describe a novel combination of ovarian follicle imaging with BCB as intra-vital contrasting medium using MSOT technology. The volumetric optoacoustic scanning (planar imaging plus Z-translation) provided suitable anatomical landmarks, and multi-wavelength acquisition allowed spectral resolution of the contrast agent (BCB). The anatomic scans using single-wavelength optoacoustic images and three-dimensional acquisitions distinctly show the follicular antrum and theca internal layers (figure 3; electronic supplementary material, movie S1), allowing individual follicles to be easily identified. The segmentation and volumetric evaluation of the follicles from anatomic data (as carried out in the ultrasonic evaluation of ovaries in clinical cases) can also be achieved using the MSOT data [4,42]. However, such evaluations are beyond the scope of the current article and are anyway redundant and insufficient in view of the availability of superior molecular information (BCB contrast) provided by MSOT.

Ovarian follicles were validated by a state-of-the-art SPIM system specifically designed for ovarian follicle imaging. Clearly distinguishable COCs protruding into the follicular

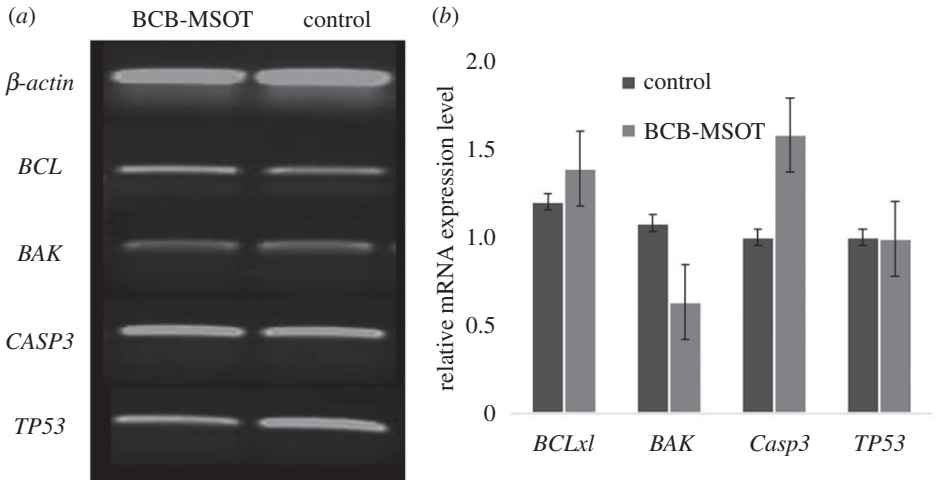

Figure 7. The reverse transcription PCR of (*a*) apoptosis-associated and stress-associated genes in MSOT-scanned oocytes (exposure 5–20 min). (*b*) The statistical significances for tests conducted with β-actin, BCL, BAK and TP53—no significant DNA damage due to BCB and/or MSOT scanning is observed.

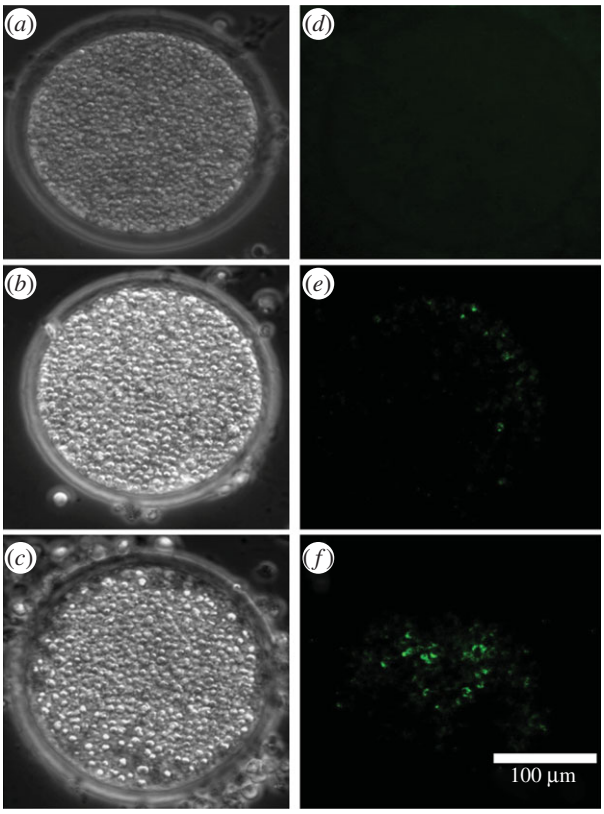

Figure 8. DNA fragmentation detection (bright-field images) by TUNEL assay: (*a*) porcine oocyte with no detectable DNA fragmentation, (*b*) BCB +ve porcine oocyte with DNA fragmentation and (*c*) control oocyte with DNA fragmentation. The corresponding fluorescent channel images of (*a–c*) are shown (*d–f*) on the same scale.

antrum of several antral and Graafian follicles were measured at 40–110 µm, and their correlation with the developmental stage of the follicles was as described by others [33] (electronic supplementary material, figure S1). SPIM imaging coupled with the cryosection and histological (H&E stained) images provided a suitable measure to determine the efficacy of the BCB contrast-enhanced MSOT imaging protocol.

The MSOT system has lower imaging resolution compared to microscopy but has the advantage of being non-destructive, unlike SPIM and histological analyses. The high spatial resolution and excellent contrast offered by BCB contrast-enhanced MSOT imaging provide quantitative anatomical information similar to that obtained by ultrasonic measurements commonly used in animal studies [33] and clinical practice [4]. Furthermore, the functional capability of MSOT as an imaging modality allows visualizing the presence (or absence) of BCB contrast without disrupting the follicle, opening up exciting new possibilities in molecular imaging for ART. Maintaining oocyte viability was one of the most important criteria for our study and defined the choice of BCB as a contrast medium and MSOT as a non-ionizing imaging modality. MSOT imaging added an extra few hours to the processing of COC and *in vitro* culture. The RT-PCR and embryo development assay were done to see if the additional steps have any detrimental effect on the oocyte quality. However, we found no contraindications. Parthenogenetic activation and embryo development indicated that the imaging was harmless and analysis of DNA fragmentation, and the expression of important apoptosis-related genes indicated no apparent damage to the oocytes. Our investigation provides further support for the use of BCB as a safe labelling agent for oocyte selection and demonstrates the applicability of MSOT in *in vitro* embryo production.

There is immense scope for improving ovarian imaging techniques, as existing methods provide only crude information with questionable predictive value. Oocyte quality is certainly an important factor determining the outcome of ART procedures, but so far it has not been possible to test oocyte quality within a follicle. We therefore anticipate that a non-destructive method that reliably predicts the quality of the developing oocyte inside a follicle will be of great benefit. As illustrated in the current article, an approach for functional oocyte and embryo assessment by ovarian imaging with the use of an exogenous contrast agent can indeed be a key new technology for artificial reproduction.

The current study is a step beyond the conventionally practiced ultrasound guided antral follicle count and the proxy biochemical tests used for predicting ovarian reserve. The proposed methodology takes into account the quality, the competence and the developmental potential of the oocyte residing in the follicles within the ovary. Recent advancements in MSOT technology have allowed non-invasive assessment of intestinal wall [43], transvaginal imaging of ovaries [44] and transrectal imaging of prostate [45]. These technological

progresses in system design will indeed be helpful in translating our imaging protocol to clinics. Future development of the approach will open new dimensions in follicular imaging delivering useful anatomical, functional and molecular information without hampering the integrity of the follicle. Possible applications include diagnosis of follicular cysts, empty follicle syndrome and developmental studies. The poor quality of retrieved oocytes due to improper timing of oocyte retrieval is an important factor in the relatively low success rate of human IVF. *In vivo* visualization of oocytes *in situ* could help practitioners to make informed decisions about timing oocyte retrieval.

4. Experimental section

The materials and methods are detailed in the electronic supplementary material. Additional results (electronic supplementary material, table S1 and figures S1 and S2) supporting the claims made in the paper are included in the electronic supplementary material.

Ethics. All procedures involving animal care and experimentation were conducted according to the guidelines of Helmholtz Zentrum München and the government of Upper Bavaria and complied with German federal and international laws and regulations.

Data accessibility. Additional details of the methods and datasets used are included in the electronic supplementary material document. The flythrough videos of entire imaging datastacks for MSOT and SPIM are available as electronic supplementary material.

Authors' contributions. R.D. and S.M. jointly conceived the idea of the imaging protocol, designed and conducted experiments; they contributed equally to the project. S.M. conducted the optoacoustic (OA) measurement, and developed/improved the imaging and image analysis algorithms. R.D. participated in the OA studies and was responsible for *in vitro* embryo cultures and biological assays. H.C.A.L. and D.R. developed and conducted the experiments using the SPIM system. R.D., S.M. and H.C.A.L. executed the histological imaging and validation steps. D.R., A.K., A.S. and T.R. critically reviewed and validated the findings. A.S. and D.R. supported and supervised the project. R.D., S.M., A.K. and D.R. participated in writing and revising the manuscript.

Competing interests. The authors declare no conflict of interest.

Funding. R.D. and S.M. acknowledge DAAD (PhD Scholarships) for the funding support. And this study was supported by Deutscher Akademischer Austauschdienst (grant no. 91540909).

Acknowledgements. We thank S. J. Ford and R. Phaltane for the productive discussions, V. Gujrati for his suggestions and proofreading the manuscript. We would like to thank Steffen Löbnitz for his help in collecting samples.

References

1. Tal R, Seifer DB. 2017 Ovarian reserve testing: a user's guide. *Am. J. Obstet. Gynecol.* **217**, 129–140. (doi:10.1016/j.ajog.2017.02.027)
2. Fransisco K. 2016 Assisted reproductive technology. In *Encyclopedia of family studies* (ed. CL Shehan). Hoboken, NJ: Wiley. (doi:10.1002/9781119085621.wbefs435)
3. Hiremath PS, Tegnoor JR. 2013 Follicle detection and ovarian classification in digital ultrasound images of ovaries. In *Advancements and breakthroughs in ultrasound imaging* (ed. GPP Gunarathne). London, UK: InTech Open. (doi:10.5772/56518)
4. Krivanek A, Sonka M. 1998 Ovarian ultrasound image analysis: follicle segmentation. *IEEE Trans. Med. Imaging* **17**, 935–944. (doi:10.1109/42.746626)
5. Zheng H, Chen X-L, Zhu C-Q, Li D-H, Chen Q-Y, Xu J-G. 2000 Brilliant cresyl blue as a new red region fluorescent probe for determination of nucleic acids. *Microchem. J.* **64**, 263–269. (doi:10.1016/S0026-265X(00)00015-1)
6. Preložnik-Zupan I, Černelč P, Žontar D. 2000 Reticulocyte analysis using light microscopy and two different flow cytometric procedures. *Pflugers Arch.* **440**, R185–R187. (doi:10.1007/s004240000058)
7. Pereira GR, Lorenzo PL, Carneiro GF, Bilodeau-Goeseels S, Kastelic JP, Esteller-Vico A, Lopez-Bejar M, Liu IKM. 2014 Selection of developmentally competent immature equine oocytes with brilliant cresyl blue stain prior to in vitro maturation with equine growth hormone. *Zygote* **22**, 500–504. (doi:10.1017/S096719941200072X)
8. Manjunatha BM, Gupta PSP, Devaraj M, Ravindra JP, Nandi S. 2007 Selection of developmentally competent buffalo oocytes by brilliant cresyl blue staining before IVM. *Theriogenology* **68**, 1299–1304. (doi:10.1016/j.theriogenology.2007.08.031)
9. Katska-Ksiazkiewicz L, Opiela J, Ryńska B. 2007 Effects of oocyte quality, semen donor and embryo co-culture system on the efficiency of blastocyst production in goats. *Theriogenology* **68**, 736–744. (doi:10.1016/j.theriogenology.2007.06.016)
10. Su J, Wang Y, Li R, Peng H, Hua S, Li Q, Quan F, Guo Z, Zhang Y. 2012 Oocytes selected using BCB staining enhance nuclear reprogramming and the *in vivo* development of SCNT embryos in cattle. *PLoS ONE* **7**, e36181. (doi:10.1371/journal.pone.0036181)
11. Stanton RC. 2012 Glucose-6-phosphate dehydrogenase, NADPH, and cell survival. *IUBMB Life* **64**, 362–369. (doi:10.1002/iub.1017)
12. Mirshamsi SM, KaramiShabankareh H, Ahmadi-Hamedani M, Soltani L, Hajarian H, Abdolmohammadi AR. 2013 Combination of oocyte and zygote selection by brilliant cresyl blue (BCB) test enhanced prediction of developmental potential to the blastocyst in cattle. *Anim. Reprod. Sci.* **136**, 245–251. (doi:10.1016/j.anireprosci.2012.11.002)
13. Razansky D, Distel M, Vinegoni C, Ma R, Perrimon N, Köster RW, Ntziachristos V. 2009 Multispectral opto-acoustic tomography of deep-seated fluorescent proteins in vivo. *Nat. Photonics* **3**, 412–417. (doi:10.1038/nphoton.2009.98)
14. Mandal S, Dean-Ben XL, Burton NC, Razansky D. 2015 Extending biological imaging to the fifth dimension: evolution of volumetric small animal multispectral optoacoustic tomography. *IEEE Pulse* **6**, 47–53. (doi:10.1109/MPUL.2015.2409103)
15. Ripoll J, Koberstein-Schwarz B, Ntziachristos V. 2015 Unleashing optics and optoacoustics for developmental biology. *Trends Biotechnol.* **33**, 679–691. (doi:10.1016/j.tibtech.2015.08.002)
16. Ermolayev V, Dean-Ben XLXL, Mandal S, Ntziachristos V, Razansky D. 2015 Simultaneous visualization of tumour oxygenation, neovascularization and contrast agent perfusion by real-time three-dimensional optoacoustic tomography. *Eur. Radiol.* **26**, 1–9. (doi:10.1007/s00330-015-3980-0)
17. Viator JA, Sutovsky P, Weight RM. 2008 Detection of dilute sperm samples using photoacoustic flowmetry. In *Photons Plus Ultrasound: Imaging and Sensing 2008: The Ninth Conference on Biomedical Thermoacoustics, Optoacoustics, and Acousto-optics*.
18. Tzoumas S, Deliolanis N, Morscher S, Ntziachristos V. 2013 Un-mixing molecular agents from absorbing tissue in multispectral optoacoustic tomography. *IEEE Trans. Med. Imaging* **33**, 48–60. (doi:10.1109/TMI.2013.2279994)
19. Mandal S, Dean-Ben XL, Razansky D. 2016 Visual quality enhancement in optoacoustic tomography using active contour segmentation priors. *IEEE Trans. Med. Imaging* **35**, 2209–2217. (doi:10.1109/TMI.2016.2553156)
20. Ntziachristos V, Razansky D. 2010 Molecular imaging by means of multispectral optoacoustic tomography (MSOT). *Chem. Rev.* **110**, 2783–2794. (doi:10.1021/cr9002566)
21. Ding L, Luís Deán-Ben X, Lutzweiler C, Razansky D, Ntziachristos V. 2015 Efficient non-negative constrained model-based inversion in optoacoustic tomography. *Phys. Med. Biol.* **60**, 6733–6750. (doi:10.1088/0031-9155/60/17/6733)

22. Prakash J, Mandal S, Razansky D, Ntziachristos V. 2019 Maximum entropy based non-negative optoacoustic tomographic image reconstruction. *IEEE Trans. Biomed. Eng.* **66**, 2604–2616. (doi:10.1109/TBME.2019.2892842)
23. Mandal S, Nasonova E, Deán-Ben XL, Razansky D. 2014 Optimal self-calibration of tomographic reconstruction parameters in whole-body small animal optoacoustic imaging. *Photoacoustics* **2**, 128–136. (doi:10.1016/j.pacs.2014.09.002)
24. Luke GP, Nam SY, Emelianov SY. 2013 Optical wavelength selection for improved spectroscopic photoacoustic imaging. *Photoacoustics* **1**, 36–42. (doi:10.1016/j.pacs.2013.08.001)
25. Mohammadi-Sangcheshmeh A, Soleimani M, Deldar H, Salehi M, Soudi S, Hashemi SM, Schellander K, Hoelker M. 2012 Prediction of oocyte developmental competence in ovine using glucose-6-phosphate dehydrogenase (G6PDH) activity determined at retrieval time. *J. Assist. Reprod. Genet.* **29**, 153–158. (doi:10.1007/s10815-011-9625-6)
26. Fuenzalida WJP *et al.* 2020 Challenging a preconception: optoacoustic spectrum differs from the optical absorption spectrum of proteins and dyes for molecular imaging. *Anal. Chem.* **92**, 10717–10724. (doi:10.1021/acs.analchem.0c01902)
27. Nascimento JMP, Dias JMB, Bioucas-Dias JM. 2005 Vertex component analysis: a fast algorithm to unmix hyperspectral data. *IEEE Trans. Geosci. Remote Sens.* **43**, 898–910. (doi:10.1109/TGRS.2005.844293)
28. Viswanath PSS, Weiser T, Chintala P, Mandal S, Dutta R. 2016 Grading of mammalian cumulus oocyte complexes using machine learning for in vitro embryo culture. In *2016 IEEE-EMBS Int. Conf. on Biomedical and Health Informatics, Las Vegas, NV, USA, 24–27 February 2016*, pp. 172–175. (doi:10.1109/BHI.2016.7455862)
29. Borup R, Thuesen LL, Andersen CY, Nyboe-Andersen A, Ziebe S, Winther O, Grøndahl ML. 2016 Competence classification of cumulus and granulosa cell transcriptome in embryos matched by morphology and female age. *PLoS ONE* **11**, e0153562. (doi:10.1371/journal.pone.0153562)
30. Razansky D, Buehler A, Ntziachristos V. 2011 Volumetric real-time multispectral optoacoustic tomography of biomarkers. *Nat. Protoc.* **6**, 1121–1129. (doi:10.1038/nprot.2011.351)
31. He H, Mandal S, Buehler A, Dean-Ben XLL, Razansky D, Ntziachristos V. 2016 Improving optoacoustic image quality via geometric pixel super-resolution approach. *IEEE Trans. Med. Imaging* **35**, 812–818. (doi:10.1109/TMI.2015.2497159)
32. Lin HCAH-CA *et al.* 2016 Advancing ovarian folliculometry with selective plane illumination microscopy. *Sci. Rep.* **6**, 38057. (doi:10.1038/srep38057)
33. Griffin J, Emery BR, Huang I, Peterson CM, Carrell DT. 2006 Comparative analysis of follicle morphology and oocyte diameter in four mammalian species (mouse, hamster, pig, and human). *J. Exp. Clin. Assist. Reprod.* **3**, 2. (doi:10.1186/1743-1050-3-2)
34. Pfeifer LFM, Siqueira LGB, Adams GP, Pierson RA, Singh J. 2012 In vivo imaging of cumulus-oocyte-complexes and small ovarian follicles in cattle using ultrasonic biomicroscopy. *Anim. Reprod. Sci.* **131**, 88–94. (doi:10.1016/j.anireprosci.2012.02.014)
35. Rodríguez-González E, López-Béjar M, Velilla E, Paramio MT. 2002 Selection of prepubertal goat oocytes using the brilliant cresyl blue test. *Theriogenology* **57**, 1397–1409. (doi:10.1016/S0093-691X(02)00645-3)
36. Pujol M, López-Béjar M, Paramio MT. 2004 Developmental competence of heifer oocytes selected using the brilliant cresyl blue (BCB) test. *Theriogenology* **61**, 735–744. (doi:10.1016/S0093-691X(03)00250-4)
37. Chandrakanthan V, Li A, Chami O, O'Neill C. 2006 Effects of in vitro fertilization and embryo culture on TRP53 and Bax expression in B6 mouse embryos. *Reprod. Biol. Endocrinol.* **4**, 61. (doi:10.1186/1477-7827-4-61)
38. Morita Y, Tilly JL. 1999 Oocyte apoptosis: like sand through an hourglass. *Dev. Biol.* **213**, 1–17. (doi:10.1006/dbio.1999.9344)
39. Dutta R *et al.* 2016 Non-invasive assessment of porcine oocyte quality by supravital staining of cumulus–oocyte complexes with lissamine green B. *Zygote* **24**, 418–427. (doi:10.1017/S0967199415000349)
40. ANSI. 2014 *American National Standard for Safe Use of Lasers*. See http://webstore.ansi.org/RecordDetail.aspx?sku=ANSI+Z136.1-2014.
41. Yuan YQ, Van Soom A, Leroy JLMR, Dewulf J, Van Zeveren A, de Kruif A, Peelman LJ. 2016 Apoptosis in cumulus cells, but not in oocytes, may influence bovine embryonic developmental competence. *Theriogenology* **63**, 2147–2163. (doi:10.1016/j.theriogenology.2004.09.054)
42. Kwee J, Elting ME, Schats R, McDonnell J, Lambalk CB. 2007 Ovarian volume and antral follicle count for the prediction of low and hyper responders with in vitro fertilization. *Reprod. Biol. Endocrinol.* **5**, 9. (doi:10.1186/1477-7827-5-9)
43. Knieling F *et al.* 2017 Multispectral optoacoustic tomography for assessment of Crohn's disease activity. *N. Engl. J. Med.* **376**, 1292–1294. (doi:10.1056/NEJMc1612455)
44. Salehi HS, Li H, Merkulov A, Kumavor PD, Vavadi H, Sanders M, Kueck A, Brewer MA, Zhu Q. 2016 Coregistered photoacoustic and ultrasound imaging and classification of ovarian cancer: ex vivo and in vivo studies. *J. Biomed. Opt.* **21**, 046006. (doi:10.1117/1.jbo.21.4.046006)
45. Kothapalli SR *et al.* 2019 Simultaneous transrectal ultrasound and photoacoustic human prostate imaging. *Sci. Transl. Med.* **11**, eaav2169. (doi:10.1126/scitranslmed.aav2169)